COMSOL-PV: A Unified Platform for Numerical Simulation of Solar Cells and Modules

Marco Nardone, Dept. of Environment and Sustainability, Bowling Green State University
Bowling Green, Ohio, 43403, USA, marcon@bgsu.edu

Abstract: A general approach is presented for using COMSOL Multiphysics® to simulate photovoltaic (PV) device performance and reliability. It is shown how the multi-physics, multi-scale, 2D/3D, and time-dependent capabilities make COMSOL a platform for simulating any type of PV device. Customizable physics makes this an extremely versatile tool for designing new devices and for better understanding existing technology. We use the specific example of cadmium telluride thin-film PV to demonstrate the simulation of micron size diodes with grain boundaries, solar cells, and solar modules. Insights to a mechanism of gradual power output decay over time (degradation) are also presented.

Keywords: semiconductor modeling, photovoltaic devices, solar electricity, thin-films

1. Introduction

Photovoltaic (PV) energy production is expected to continue to grow exponentially over the next several decades. Yet, a wide range of new materials and device architectures are being investigated, which suggests that there is a great deal of room for innovation and discovery. Effective simulation capabilities can help to guide such innovation. There are several free PV modeling software packages available [1] [2] [3] [4] but they have several limitations, including 1D only, no other physics coupling, no time dependence, minimal post-processing tools, etc. Some of those limitations are overcome by more sophisticated software [5] but they tend to be prohibitively expensive and do not easily couple multiple physics modes.

In this work, we provide an overview and some examples of how COMSOL Multiphysics® can serve as a unified platform for PV simulation with multi-dimensional, multi-physics, and multi-scale capabilities. Specific results are given for simulating the degradation (power output loss over time) of cadmium telluride (CdTe) thin-film devices.

The primary inputs to any PV model are the material parameters which describe the electronic and optical properties of each device layer (there are often several layers of material), the contact types, and external conditions including illumination intensity/spectrum, voltage bias (or external load), and temperature. Additional input values are required when physics modes beyond the standard semiconductor equations are employed, as described below.

The most important output is the current-voltage (IV) curve (i.e. current as a function of applied voltage) because it provides information on energy conversion efficiency, η, and several other metrics. Other outputs include quantum-efficiency (QE), which measures the ability to collect photo-generated electron-hole pairs, and capacitance-voltage (CV) properties, which help to understand certain electronic properties. All of the above outputs are macroscopic observables, but deeper investigation stems from calculating things that are difficult to measure, such as energy band diagrams and recombination rates.

PV devices have extremely large aspect ratios, with thicknesses on the order of 1-300 um and lateral dimensions of ~ 1 cm for cells and ~ 1 m for modules. In what follows we describe how COMSOL is used to calculate the above outputs at the various spatial scales, thereby simulating PV performance from nanometers to meters.

Designing PV devices and understanding how their performance changes over time requires coupling to optical, thermal, drift-diffusion-reaction physics with a time-dependent solver. We have used those tools in COMSOL to simulate device degradation [6] [7] and ion diffusion. Some examples are provided herein.

2. Use of COMSOL Multiphysics for PV

2.1 Micron-scale Modeling

The most basic use of COMSOL for PV simulation requires both the Semiconductor and Wave Optics modules. PV simulation entails determining the electrostatic potential, ϕ, electron concentration, n, and hole concentration, p, as

functions of space by solving the Poisson and continuity equations:

$$\nabla \cdot (\varepsilon_s \nabla \phi) = -\rho \qquad (1)$$

$$\frac{\partial n}{\partial t} = \frac{1}{q}\nabla \cdot \boldsymbol{J}_n - U_n + G_n \qquad (2)$$

$$\frac{\partial p}{\partial t} = \frac{1}{q}\nabla \cdot \boldsymbol{J}_p - U_p + G_p \qquad (3)$$

where q is the unit electronic charge, ε_s is the semiconductor permittivity, U_n and U_p are recombination rates, G_n and G_p are generation rates for electrons and holes, respectively, and the charge density is given by,

$$\rho = q(n - p + N_A - N_D). \qquad (4)$$

Negative and positive fixed charge, whether they be intentional dopants or impurities, are denoted by N_A and N_D, respectively.

The current densities, $\boldsymbol{J_n}$ and $\boldsymbol{J_p}$, have both drift and diffusion components given by,

$$\boldsymbol{J}_n = -q\mu_n n\nabla\phi + qD_n\nabla n \qquad (5)$$

$$\boldsymbol{J}_p = -q\mu_p n\nabla\phi - qD_n\nabla p \qquad (6)$$

where μ is the mobility and $D = \mu kT/q$ is the diffusion coefficient with Boltzmann constant k and temperature T. The total current density is $\boldsymbol{J} = \boldsymbol{J_n} + \boldsymbol{J_p}$.

The boundary conditions (BC) on the currents depend on the type of metal contacts being considered. For the case of Schottky contacts, the BC depend on the carrier concentrations and recombination velocities, S_n or S_p, at the metal/semiconductor interface according to,

$$\boldsymbol{J}_n \cdot \hat{\boldsymbol{n}} = -qS_n(n - n_0) \qquad (7)$$

$$\boldsymbol{J}_p \cdot \hat{\boldsymbol{n}} = qS_p(p - p_0) \qquad (8)$$

where $\hat{\boldsymbol{n}}$ is the unit normal at the boundary and n_0 and p_0 are the equilibrium electron and hole concentrations. The electric potential BC is $\phi = -\Phi_m + V_a$, where Φ_m is the metal work function and V_a is the applied voltage.

The above set of equations Eqs (1) – (6), is often referred to as the "semiconductor equations" and are rather challenging to solve numerically due to the magnitudes of the opposing currents involved. Either finite volume or finite element spatial discretization methods can be employed. The most reliable approach is to use the finite volume method with the Scharfetter-Gummel scheme for the continuity equations (typical in semiconductor modeling software). The stationary solver is based on Newton's method which can be set to solve the system of equations as fully coupled or segregated. Time-dependent problems are solved using the backward differentiation formulas (BDF) method and small signal analysis is used to simulate capacitance diagnostics which require the application of a small AC bias. A review of the applicable numerical methods is available in Ref. [9].

In a semiconductor, charge carriers (n and p) can be generated or lost due to recombination via various physical properties that depend on the material parameters, external conditions, and energy states (defects) available in the band gap. The reader is referred to Sze [8] for a detailed description. COMSOL's Semiconductor Module includes several built-in options for recombination mechanisms, as well as user defined functions. The pertinent mechanism for our discussion below is that of Shockley-Read-Hall,

$$U_n = U_p \propto N_t(pn - n_0p_0), \qquad (9)$$

where N_t is the concentration of defects in the gap.

Photo-generation rates, $G = G_n = G_p$, are determined by first calculating the optical electric field using the Wave Optics Module to solve Maxwell's equations in the frequency domain,

$$\nabla \times (\nabla \times \boldsymbol{E}) - k_0^2\varepsilon_r\boldsymbol{E} = 0 \qquad (10)$$

where k_0 is the wave vector. The complex refractive index $\varepsilon_r = (n_r - ik_e)^2$ is a function of wavelength (λ) and is comprised of a real part, n_r, and imaginary part, k_e, also known as the extinction coefficient. The absorption coefficient is given by $\alpha = 4\pi k_e/\lambda$. The light intensity decreases as it is absorbed and the power dissipation density, Q, can be used to calculate the generation rate, $G = Q/h\nu$, where h is Planck's constant and ν is the frequency of the electromagnetic wave. The incident light must be input as a spectrum with the intensity specified for each frequency. Port boundary conditions are

employed to specify input power and angle of incidence. Through trial and error we discovered that the most reliable method for obtaining solver convergence is to first solve the dark, equilibrium problem with a somewhat coarse mesh. Then, one can use that solution as the initial value for the illuminated model by ramping up the light intensity with a parametric sweep on a finer mesh.

The Wave Optics Module can be used to simulate design features that involve plasmonics and other optical structures. However, if a simple 1D approach will suffice for a given simulation, one can calculate the $G(x)$ using the standard exponential power decay formula [8].

When using 1D software, the typical approach is to solve the equations in only the transversal direction (main direction of current flow through the semiconductor) and assume that there are no parameter variations in the two lateral directions (parallel to flow). Hence, the 1D results are assumed to capture the average performance of an entire solar cell. That uniformity assumption breaks down, however, when there are unintentional features, such as grain boundaries and other lateral variations in polycrystalline devices, or intentional variations, such as alternating contact types in back-contacted crystalline silicon cells. In fact, even conventional crystalline cells can have lateral nonuniformity due to the formation of dislocations and preferential ion diffusion. Incorporating those features requires at least 2D modeling.

Consider the effects of grain boundaries in polycrystalline semiconductors. Grain boundaries are important because they can act as regions of high recombination and space charge density that can drastically affect the electronic properties of the device (especially when the grain size is similar to the electric field screening length) [10]. They can also act as diffusion pathways for impurity ions to flow through the device, resulting in temporal variations in electronic properties. We can simulate the effects of ion movement by coupling the semiconductor equations of Eqs. (1) – (6) with the drift/diffusion/reaction equation,

$$\frac{\partial c}{\partial t} = \nabla \cdot (\mathrm{D}_i \nabla \mathrm{c}) + \nabla \cdot (c\mu \nabla \phi) + R \qquad (11)$$

where c is the ion concentration D_i is the ion diffusion coefficient, μ is the ion mobility, and R is the reaction rate. c must be added to the charge density of Eq. (4) to complete the coupling.

One example of 2D/3D modeling with semiconductor and diffusion coupled physics is shown in Fig. 1. In that model we consider a single, cylindrical grain of a polycrystalline cadmium telluride (CdTe) thin-film solar cell, which also has cadmium sulfide (CdS) and tin oxide (SnO_2) layers, and metal contacts (not shown). The CdTe grain is surrounded by an annular grain boundary (2 nm wide) with an ion diffusion coefficient, D_i, that is five orders of magnitude greater than that of the bulk grain. Ion accumulation within the grain boundary is observed in a region where the electric field forms a valley. The movement of the ions with respect to applied bias, temperature, and illumination, along with the effects on device performance, can be calculated using this model.

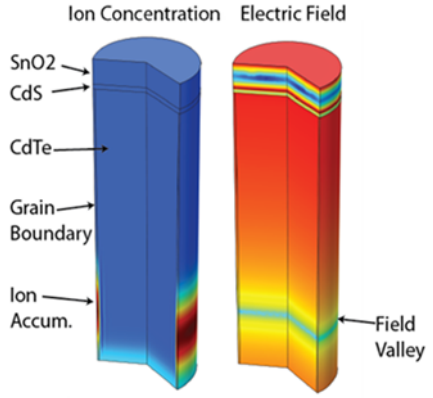

Figure 1. Model of a CdTe PV micro-diode with a cylindrical grain surrounded by an annular grain boundary. The total thickness is ~ 3 μm and the diameter is 1 μm. Left: ion concentration showing accumulation in the 2-nm wide grain boundary. Right: electric field distribution.

The electronic effects of grain boundaries are illustrated in Figs. 2 and 3, which show IV and QE curves for various levels of grain boundary recombination and charge.

2.2 Cell-scale Modeling

Given the large aspect ratio of PV cells, it is impractical to solve the semiconductor equations on the cell scale of centimeters. Instead, the fundamental physics is calculated at the micron scale and those outputs are extrapolated to the cell scale. Specifically, the current as a function of

voltage, V, temperature, T, and illumination, Γ, are calculated at the micron scale and those values are used to build an interpolating function, $j(V,T,\Gamma)$. That interpolating function is then used as an input to the cell scale model, as described next.

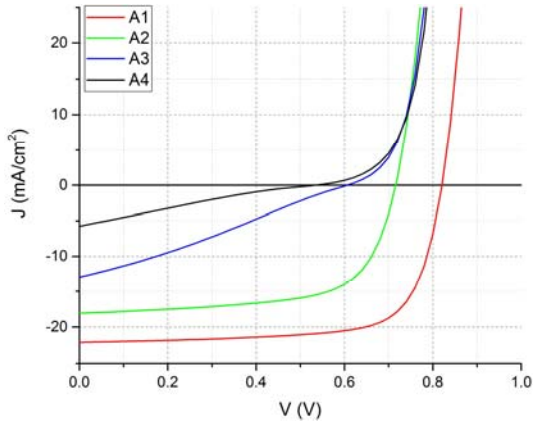

Figure 2. Current density vs. voltage curves for CdTe micro-diodes under AM1.5 illumination with various levels of grain boundary charge and recombination.

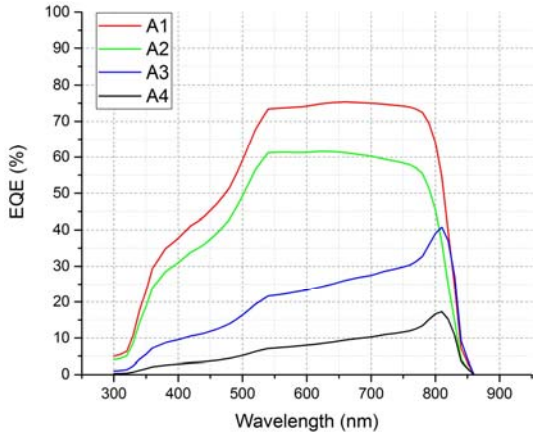

Figure 3. External quantum efficiency as a function of light wavelength for the same cells as in Fig. 2.

First consider the 1D equivalent circuit model of a thin-film solar cell shown in Fig. 3. The micro-diodes, which are in parallel to each other feed a certain amount current density per unit length (or area in 2D), $j(V,T,\Gamma)$, into the top transparent conducting oxide (TCO) layer, which has some finite sheet resistance, R_{TCO}. The metal contact on the bottom is assumed to be a perfect conductor on this scale. In the limit of infinitesimal lateral diode spacing, we obtain the current conservation equation $\nabla \cdot \boldsymbol{J} = j/d$, which provides the current density in the TCO layer and where j serves as a source term in units of A/m^2. Then using ohms law, $\boldsymbol{J} = -\sigma\nabla\phi$ we obtain,

$$-\nabla \cdot (\sigma\nabla\phi) = j/d \qquad (12)$$

where the TCO conductivity is $\sigma = 1/(d\ R_{TCO})$. The TCO thickness, d, is usually less than one micron. Eq. (12) can be solved using the Electric Currents physics mode within the AC/DC module. Boundary conditions on ϕ can be set to study any metal contact shape or location.

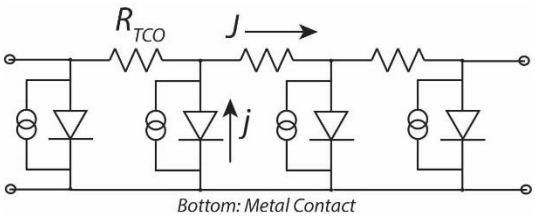

Figure 3. Equivalent circuit model of a solar cell used to derive Eq. (12).

Fig. 4 shows an example of the calculated $\phi(x, y)$ distribution for a 1-cm diameter CdTe cell, at open circuit conditions, with the left half shaded and the right half fully illuminated with AM1.5 radiation at 1 sun intensity. The contact is located around the outer edge of the cell.

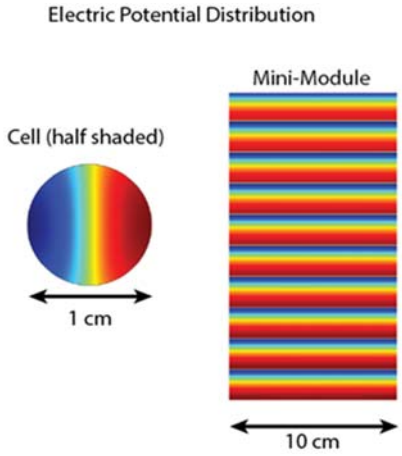

Figure 4. Calculated electric potential distributions of a cell and module. Left: CdTe solar cell under open circuit that is half shaded (color range of 0.83 to 0.87 V from blue to red). Right: CdTe module under short

circuit that is uniformly illuminated (color range of 0 to 0.12 V from blue to red).

2.3 Module-scale Modeling

There are basically two types of modules depending on how the individual cells are electrically connected: 1) soldered; and 2) monolithically integrated. We will focus on the latter since that is how thin-film PV modules are constructed. These modules are made by depositing the active materials over the entire surface of the substrate then scribing the contacts using a laser or other means. A simplified diagram of a module section is shown in Fig. 5. The dashed lines in Fig. 5 indicate different current domains, not breaks in the material. Typical scribe widths (δ_1, δ_2, δ_3) are on the order of 100 μm and the active region is $\delta_0 \sim 1$ cm.

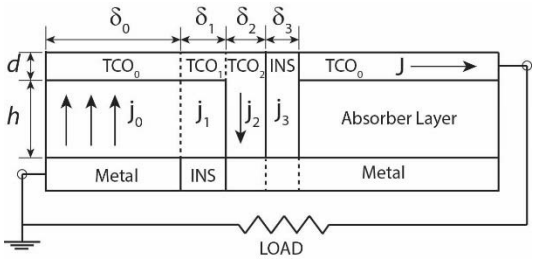

Figure 5. Monolithic module schematic with essential features for simulation. Dashed lines indicate current domains, not material breaks. Light is incident from the top.

Simulation of a monolithic module is similar to that of a cell in that we ultimately solve Eq. (12), but now we have to deal with four different current source domains, as indicated by the lower case *j*'s in Fig. 5. j_0 is the same micro-diode current $j(V,T,I)$, discussed in the cell model. In the other current domains, $j_1 = j_3 = 0$, and j_2 is an ohmic current, $j_2 = -V_2/(h\ d\ R_{TCO})$, where V_2 is the voltage drop across the absorber layer thickness h.

In addition to the four current domains the top and bottom layers need to be properly coupled. That is accomplished by setting up two components in the model, one for the top and one for the bottom, each with the appropriate geometry. Continuous vertical current flow is facilitated through a general extrusion function between the two components. An example of the potential distribution in the TCO layer of a module under illumination and short circuit conditions is shown in Fig. 4.

Important features of this finite element modeling approach for both cells and modules is that we can simulate devices of any shape and contact layout, investigate nonuniformity effects, and couple with thermal physics to build an electro-thermal model. The last point is particularly crucial for studying how modules degrade due to hot spots and shunts.

3. Theory of CdTe/CdS Junction Degradation

PV devices can degrade in several ways but here we will focus on the gradual efficiency decline of CdTe cells. We consider a mechanism based on observations [11] that excess charge carriers (whether photo- or bias-induced) are drivers of degradation in CdTe solar cells. Similar concepts have been extensively investigated for other types of semiconductors (see the review in [12]). From this perspective, excess charge carriers cause new defects to form, which increases recombination (see Eq. (9)) and alters the built-in field. In turn, those changes affect charge carrier concentrations and a feedback loop is established. In its simplest form, the defect (N_t) generation rate is linearly proportional to the concentration of nonequilibrium charge carriers. Hence, the rate equation is given by,

$$\frac{\partial N_t}{\partial t} = \alpha n(N_t) - \beta N_t \qquad (13)$$

where α and β are, respectively, defect creation and annihilation rates, and n can represent either non-equilibrium electron or hole concentrations. The term with β accounts for annealing effects that lead to saturation or reversal of defect formation. Both α and β are material parameters that are temperature activated and depend on the type of defect being considered. For example, $\alpha = \nu_0 exp(-E_a/kT)$, with activation energy E_a, characteristic frequency ν_0.

Given the mechanism described by Eq. (13), the defect concentration becomes a function of space and time, $N_t = N_t(\boldsymbol{x},t)$; hence, the performance metrics vary with time. The proper way to predict the outcome is to solve the coupled set of equations, including the semiconductor

equations of Eqs. (1) – (6) with Eq. (13), using an explicit time-dependent solver. Eq. (13) is included by employing COMSOL's General Form PDE module. Using this method, one can simulate stress under varying conditions of voltage bias, light, and temperature (stress conditions can also be made functions of time).

4. Results

Our initial results [7] demonstrate the effects of defect generation according to Eq. (1). The model predictions were compared to a set of six cells that were fabricated and stressed at the National Renewable Energy Laboratory (NREL). Results are presented in Fig. 6, which shows how the efficiency changes over time while the cells are exposed to light and temperatures of 65°C (stress test).

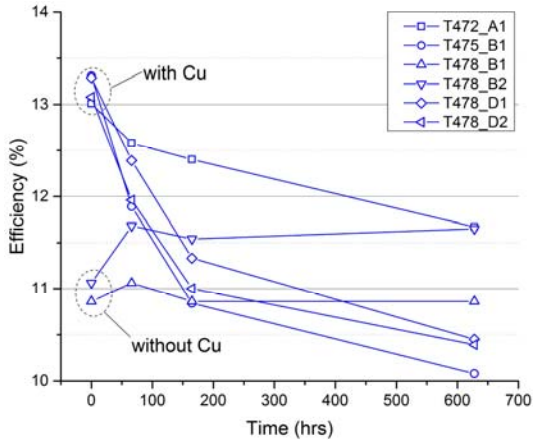

Figure 6. Efficiency as a function of time for CdTe cells with and without copper stressed under AM1.5G, 1-sun light, open-circuit, 65 °C. From [7].

Our simulation approach can predict how the key performance metrics of open-circuit voltage, V_{oc}, short circuit current, J_{sc}, fill factor, FF, and η change over time. A comparison of the model predictions to the experimental data is provided in Fig. 7. The results indicate that typically observed degradation modes are fairly well predicted by our model. A defect activation energy of E_a = 1 eV was used to fit the results, providing insights to the possible microscopic defect mechanisms underlying the observed degradation.

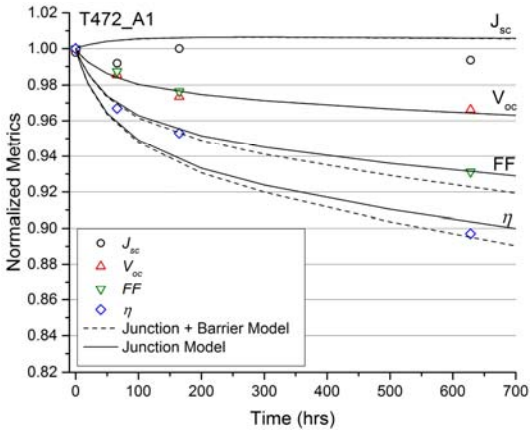

Figure 7. Normalized performance metrics as functions of time for cell T472_A1. Points are data, solid lines are model fits with junction degradation only (E_a=1 eV), dash lines include back barrier effect. From [7].

5. Conclusions

In conclusion, we have provided an overview of how COMSOL Multiphysics® can be used to simulate PV devices from the nanometer to meter scale. Modeling in more than 1D allows for the inclusion of nonuniformity effects and novel design features. Time-dependent modeling and coupling to other physics modes also allows one to simulate how device performance changes over time and how it varies with changing environmental conditions. Our specific example that employs those features indicates that the degradation of CdTe thin-film devices could be affected by defect generation caused by non-equilibrium charge carriers. In general, the overall approach presented herein can be used to simulate the performance and reliability of any PV device.

Further work will include integrating the PV simulation tool with LiveLink™ for MATLAB® and building baseline models for the most prevalent PV technologies. The development of fully coupled electro-thermal models of modules with nonuniformities will also be undertaken, as well as further study of pertinent degradation mechanisms.

6. References

[1] P. Basore, Numerical modeling of textured silicon solar cells using PC-1D, *IEEE Transaction on Electronic Devices,* **37**, no. 2, p. 337 (1990).

[2] M. Burgelaman, P. Nollet and S. Degrave, Modelling polycrystalline semiconductor solar cells, *Thin Solid Films*, **361**, no. 21, pp. 527-532 (2000).

[3] S. J. Fonash, AMPS-1D User Maual, University Park, PA: The Pennsylvania State University (1997).

[4] Y. Liu, Y. Sun and A. Rockett, "A new simulation software of solar cells--wxAMPS," *Solar Energy Materials and Solar Cells*, **98**, pp. 124-128 (2012).

[5] Synopsis, "Sentaurus Device Overview," [Online]. Available: http://www.synopsys.com/tools/tcad/devicesimulation/Pages/SentaurusDevice.aspx. [Accessed February 2014].

[6] M. Nardone, Towards understanding junction degradation in cadmium telluride solar cells, *Journal of Applied Physics*, **115**, p. 234502 (2014).

[7] M. Nardone and D. S. Albin, Degradation of CdTe Solar Cells: Simulation and Experiment, *IEEE Journal of Photovoltaics*, **5**, no. 3, pp. 962-967 (2015).

[8] S. Selberherr, *Analysis and Simulation of Semiconductor Devices*, New York: Springer Verlag (1984).

[9] S. M. Sze and K. K. Ng., *Physics of Semiconductor Devices*, New York: John Wiley & Sons (2006).

[10] H. J. Moller, *Semiconductors for Solar Cells*, Boston: Artech House (1993).

[11] R. Harju, V. G. Karpov, D. Grecu and G. Dorer, Electron-beam induced degradation in CdTe photovoltaics, *Journal of Applied Physics*, **88**, no. 4, pp. 1794-1801 (2000).

[12] D. Redfield and R. H. Bube, *Photoinduced Defects in Semiconductors*, Cambridge: Cambridge University Press (1996).